Accepted by the Journal of Building Physics (2007)

Microstructure and Thermal Conductivity of Hydrated Calcium Silicate Board Materials

Chi T. Do, Dale P. Bentz[1], and Paul E. Stutzman
Building and Fire Research Laboratory
National Institute of Standards and Technology
Gaithersburg, MD USA 20899-8615

Abstract

The thermal conductivity of a porous material is controlled by the thermal conductivities of its components and their spatial arrangement within the composite structure, e.g., the material's microstructure. In this paper, the relationships between thermal conductivity and microstructural parameters such as porosity and pore size are examined for two calcium silicate boards of different densities. Thermal conductivities are measured from room temperature to 400 °C using a transient plane source technique, for both the as-received boards and for a corresponding set of boards that were first heated to and held at 1000 °C for at least 4 h. Microstructure is characterized by the measurement of the boards' bulk and powder densities and an assessment of pore size based on scanning electron microscopy. The experimentally measured thermal conductivities are then compared to those predicted by three previously presented theories for porous materials. A better agreement is observed between the experimental values and two of the three theories. Aging the boards at 1000 °C has a small but significant effect on thermal conductivity, decreasing the room temperature values but increasing the 400 °C ones.

Keywords: Building technology; microstructure; porosity; radiation; thermal conductivity.

Introduction

In recent years, a variety of low-density calcium silicate-based building material products have been developed for high-temperature insulation and fire resistive material (FRM) applications. Such products typically exhibit a high degree of thermal stability, as characterized by minimal mass loss (10 % to 15 %) and thermal expansion/shrinkage (generally less than 2 %) upon exposure to temperatures on the order of 1000 °C. The hygral properties [1], the chemical and mineralogical composition [2], and the room temperature thermal conductivity as a function of moisture content [3; 4] of such calcium silicate insulation boards have been previously presented. In the current study, the focus will be three-fold: 1) investigation of the thermal conductivity of these materials as a function of temperature from room temperature to 400 °C, 2) microstructural characterization of their porosity and typical pore sizes, and 3) application of three different previously developed theories [5-7] to relate thermal conductivity to these measured microstructure characteristics.

[1] Author to whom correspondence should be addressed, (301)975-5865, Fax: (301)990-6891, dale.bentz@nist.gov

Experimental

Density Measurements

Hydrated calcium silicate boards were provided by their manufacturer in a convenient size of 150 mm by 150 mm by 25 mm. Their bulk densities were determined by separate measurements of sample mass and physical dimensions; values are provided in Table 1. It should be noted that the manufacturer's quoted densities correspond very closely to the values determined for the specimens after being exposed to 1000 °C. About 50 g of each material was ground to a powder and the powder density determined using a standard test method normally employed for determining the density of hydraulic cement powders [8], using isopropanol as the measuring solution. The powder density measurement was performed on two separate samples from each material and the average value reported (Table 1). The measured powder densities of the original materials of 2540 kg/m^3 to 2550 kg/m^3 compare favorably with a previously published value of 2541.5 kg/m^3 with a standard deviation of 26.6 kg/m^3 for a similar material [1]. After heating to 1000 °C, no significant change was observed in the materials' **powder** density.

Table 1. Densities for the two calcium silicate-based FRMs.

Material Designation	**Manufacturer's Quoted Density (kg/m^3)**	**Measured Density (kg/m^3)[9]**	**Measured Density after 1000 °C Exposure (kg/m^3)**	**Powder Density (kg/m^3)[8]**
L	288	339 ± 6.5[a]	288 ± 15[b]	2540 ± 10[a]
M	449	506 ± 1.2[a]	445 ± 23[b]	2550 ± 10[a]

[a]Standard deviation from two replicate measurements.
[b]Expanded uncertainty with a coverage factor of 2 [10].

Microstructure Characterization

Microstructure characterization was performed using a scanning electron microscope (SEM) in back-scattered electron (BSE) mode. The general epoxy impregnation procedure developed by Struble and Stutzman [11] for cement-based materials was employed to penetrate and fill the (larger) pores in the FRM materials. Specimens 25 mm by 12 mm by 12 mm were cut from larger boards and immersed (under vacuum) in a low-viscosity epoxy. A few drops of hardener were then added to the epoxy and curing was conducted overnight at 60 °C to 80 °C. The hardened specimen was then polished with a series of diamond polishing pastes of different finenesses and carbon coated for viewing in the SEM. Images from two different orientations of the boards in the epoxy matrix were collected to examine possible material anisotropy.

The obtained SEM images were imported into the ImageJ[2] image processing PC software package [12], where physical measurements of the two-dimensional sizes of individual "pores" were made. Typically, 100 individual pores were measured for each FRM material.

[2] Certain commercial products are identified in this paper to specify the materials used and procedures employed. In no case does such identification imply endorsement by the National Institute of Standards and Technology, nor does it indicate that the products are necessarily the best available for the purpose.

Stereological principles were then applied to compare these two-dimensional measurements to those expected for various three-dimensional pore geometries [13].

Thermal Conductivity Measurements

Thermal conductivity measurements were performed on a pair of nominally 75 mm by 63 mm by 25 mm thick specimens of each FRM using a Hot Disk Thermal Constants Analyzer[2] equipped with a high temperature furnace [14; 15]. A typical testing cycle for a set of specimens consisted of the following measurement and aging temperatures: room temperature (23 °C), 100 °C, 200 °C, 400 °C, followed by heating in a separate high temperature furnace to 1000 °C for at least 4 h (to simulate a fire exposure), then measurements at 400 °C, 200 °C, 100 °C, and finally room temperature. At each measurement temperature, typically 8 individual measurements of the thermal conductivity were made using the Hot Disk technique. For each measurement, a power of 0.08 W was applied for a measurement time period of 320 s. For the room temperature measurements, a sensor consisting of a nickel wire spiral encased in Kapton was employed, while for the measurements conducted in the furnace, the nickel sensor was encased in mica. Typically, a one hour waiting period was employed between measurements on a given sample at a given temperature. Additionally, for all of the measurements conducted in the furnace, it was necessary to allow a minimum of four hours for the specimens to come to an assumed equilibrium with respect to mass (water) loss and energy redistribution through the specimen thickness before performing the thermal conductivity measurements in order to obtain values that were stable over time. At room temperature, measurements were also performed on the original specimens using the anisotropic module of the Hot Disk computer software to investigate possible anisotropy in the thermal conductivity of these FRMs. In general, the radial and axial thermal conductivities determined using this module were within 10 % of one another.

Theoretical

Many theories have been presented previously for predicting the thermal conductivity of a porous material based on its microstructural parameters (such as porosity and pore size) and the thermal conductivities of its solid and "porous" components. Three of the more detailed theories that will be considered here are those of Russell [5], Frey [6], and Bruggeman [7]. For the theory of Russell, the thermal conductivity of the porous material, k_{Russell}, is given by [5]:

$$k_{Russell} = k_{solid} \frac{\nu p^{2/3} + 1 - p^{2/3}}{\nu (p^{2/3} - p) + 1 + p - p^{2/3}} \tag{1}$$

where
k_{solid} = thermal conductivity of the solid material,
$\upsilon = k_{\text{pore}}/k_{\text{solid}}$,
k_{pore} = thermal conductivity of the pores in the porous material = f(k_{cond}, k_{rad}),
p = porosity = $(\rho_{\text{powder}} - \rho_{\text{material}})/\rho_{\text{powder}}$,
ρ_{powder} = density of the solid material present in the porous material (ground to a powder for instance, see Table 1), and
ρ_{material} = density of the porous material (see Table 1).

The theory of Frey involves the same variables as that of Russell and can be written as [6]:

$$k_{Frey} = k_{solid} \frac{\nu(1-p^{1/3}+p)+p^{1/3}-p}{\nu(1-p^{1/3})+p^{1/3}} \tag{2}$$

Finally, the theory of Bruggeman can be written as [7]:

$$k_{Bruggeman} = k_{solid}[\nu + (1-p)(1-\nu)(\frac{k_{Bruggeman}}{k_{solid}})^{1/3}] \tag{3}$$

While equations (1) and (2) are directly solvable for k_{Russell} and k_{Frey}, respectively, a solution for $k_{\text{Bruggeman}}$ in equation (3) can be obtained by an iterative approach. Here, the initial "guess" values for applying an iterative method solution to equation (3) are supplied by the values of k_{Russell} obtained from equation (1). Convergence is then typically achieved within eight iterations of equation (3).

In the above equations, there are two considered contributions to the conductivity of the pores within the porous FRM: conduction and radiation; convection within (through) the pores is not considered in these theories. The conduction contribution is simply considered by using tabulated values for the thermal conductivity of air as a function of temperature [16; 17]. For radiation, for **spherical** pores, the theory developed by Loeb can be used to estimate the radiation contribution to the overall pore thermal conductivity as follows [18]:

$$k_{rad} = \frac{16}{3} r\sigma E T^3 \tag{4}$$

where
r = pore radius,
σ = Stefan-Boltzmann constant [5.669 x 10^{-8} W/($m^2 \cdot K^4$)],
E = emissivity of solid material (assumed to be 0.9 here), and
T = absolute temperature (K). In [18], a similar equation is developed for **laminar** and **cylindrical** pores, where the factor of (16/3) used for spherical pores is replaced by a factor of 8 and the radius of the pore, r, is replaced by one half of the largest (gap) dimension in the direction of heat flow. For this study, this largest dimension was estimated based on the analysis of the SEM images for each FRM and the factor of 8 was employed in equation (4), thus representing the ellipsoidal pores observed to be present in the FRM as cylinders. Assuming that the conduction and radiation contributions are acting in parallel, these two components of the pore conductivity are simply added together to obtain a final value at any given temperature.

Results and Discussion

Microstructure Characterization

The theories presented in equations (1) to (4) require the porosity and some measure of the pore size of the FRMs. The measured bulk and powder densities of the two FRMs were used

to compute their porosities; the results are provided in Table 2. Both materials undergo a small increase in porosity upon heating to 1000 °C.

Table 2. Computed porosities (from densities) of the two FRMs.

Material	Room Temperature Porosity (%)	Porosity after Exposure to 1000 °C (%)
L	86.7 %	88.7 %
M	80.2 %	82.5 %

Figure 1 provides an example SEM image of FRM L. The material is seen to consist of a randomly packed arrangement of closed cell fibrous structures. The individual "cells" are clearly ellipsoidal in shape as opposed to being simple spheres. More information on the dimensional characteristics of these ellipsoids was inferred from comparing 2-D measurements of the distribution of mean cell tangent diameters to previously tabulated intersection probabilities for different particle geometries [13]. Specifically, the measured results for the two FRMs were compared to those previously determined for ellipsoidal particles of various aspect ratios. The results for FRMs L and M are presented in Figures 2 and 3, respectively. It can be seen that the experimentally measured data is most similar to that for 3-D ellipsoidal particles with an aspect

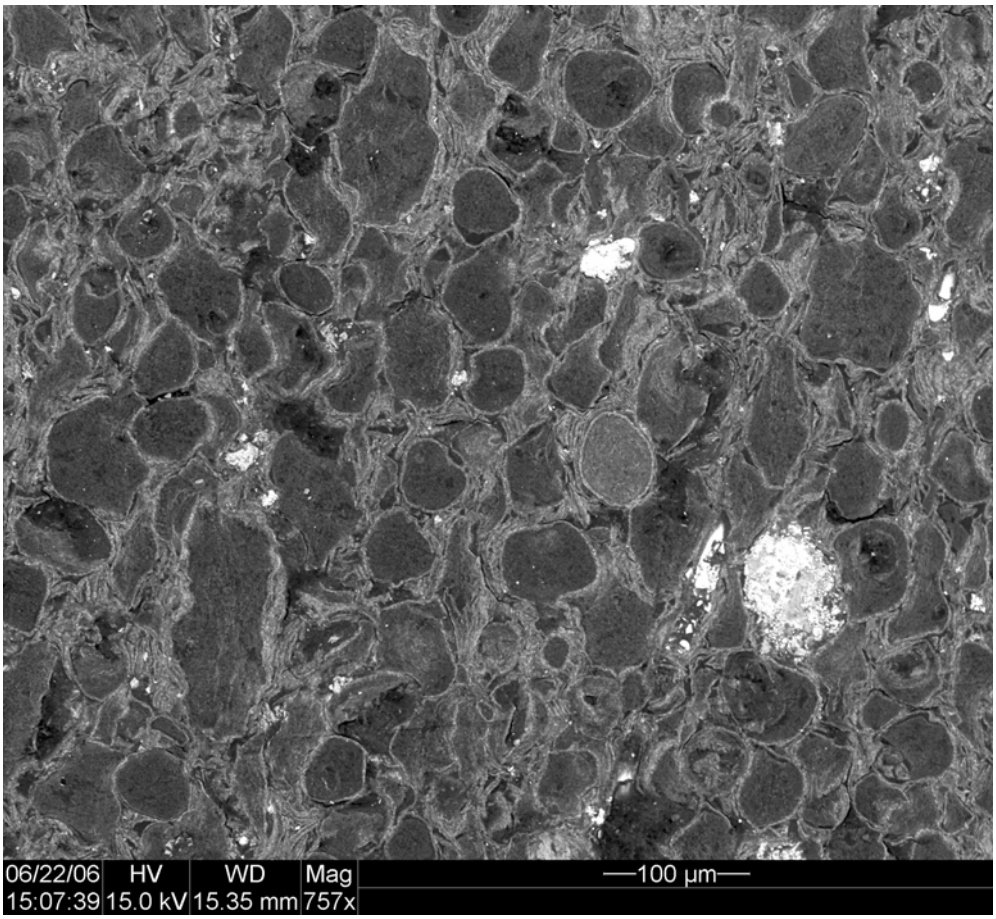

Figure 1. SEM BSE image of one of the hydrated calcium silicate board FRMs. Scale bar indicates 100 µm length. Brighter regions correspond to calcium silicate solids while darker regions correspond to air-filled or epoxy-filled pores.

ratio of either 1:2:5 or 1:3:10, choosing from the limited number of sets of analytical data presented in [13]. From images such as that in Figure 1, the maximum pore dimensions for FRMs L and M were determined to be 95 μm and 108 μm, respectively. These values will be used in the modified form of equation (4) to determine the radiation contribution to overall thermal transfer in the (represented as cylindrical) pores within the FRM materials.

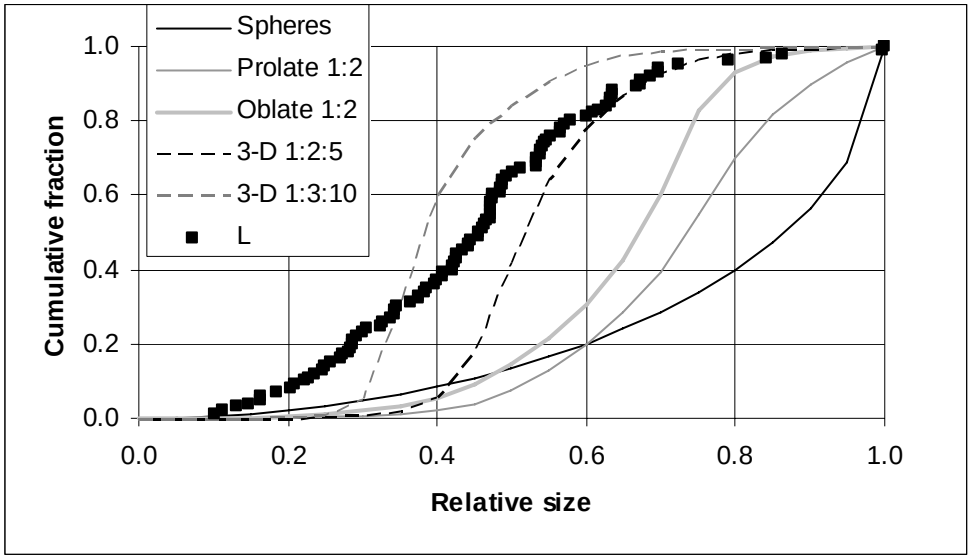

Figure 2. Cumulative probability vs. mean tangent cross-section diameter for ellipsoidal particles of various indicated aspect ratios [13] along with measurements obtained from a two-dimensional SEM/BSE image of FRM L. All sizes are scaled to the maximum size (mean tangent cross-section diameter) present in each system [13].

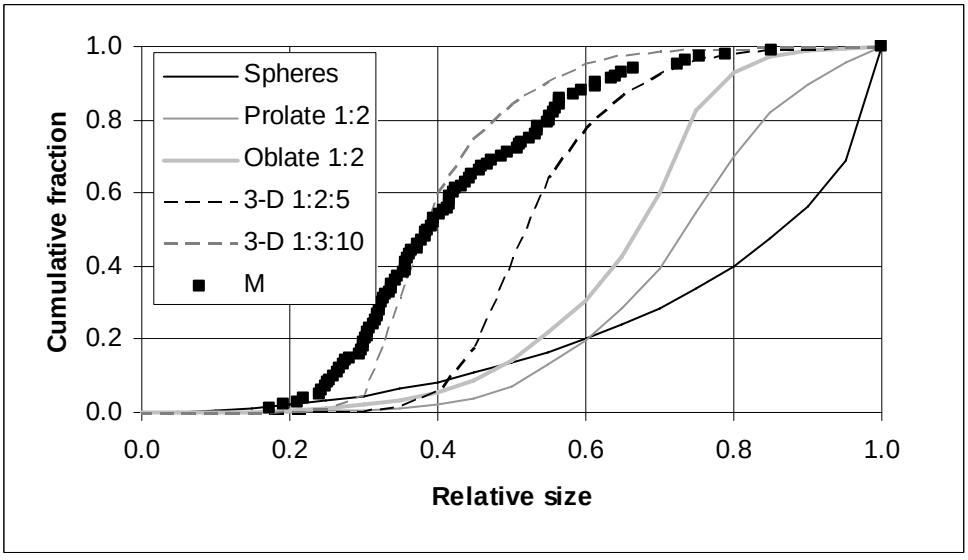

Figure 3. Cumulative probability vs. mean tangent cross-section diameter for ellipsoidal particles of various indicated aspect ratios [13] along with measurements obtained from a two-dimensional SEM/BSE image of FRM M. All sizes are scaled to the maximum size (mean tangent cross-section diameter) present in each system [13].

SEM images were also obtained of the FRMs after exposure to 1000 °C temperatures. Example images are provided in Figure 4 for FRM L at two different magnifications. Two features are worth noting in comparing the images in Figure 4 to the one of the original material provided in Figure 1. First, at the millimeter to sub-millimeter scale, some cracking of the material has occurred during the high temperature exposure. Second, there is some evidence in the higher magnification image in Figure 4 that some of the material "filling" in the microstructure between the "fibers" has collapsed or been replaced by porosity. Both of these changes might be expected to increase radiation transfer and thus also increase the effective thermal conductivity of the exposed materials at higher temperatures, relative to the original ones.

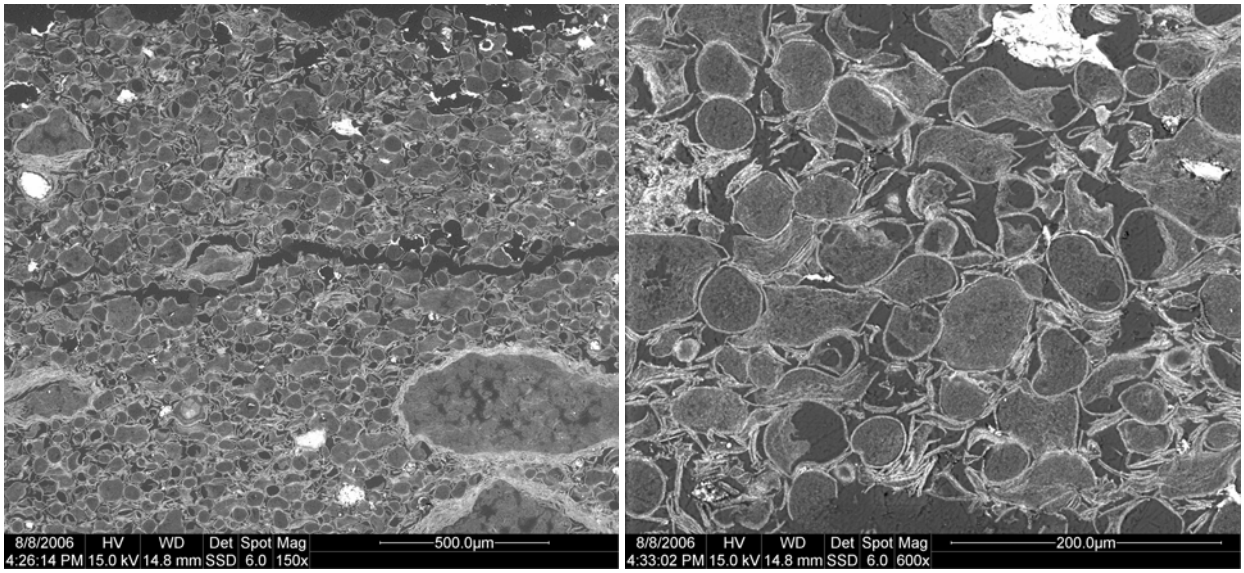

Figure 4. SEM BSE images of one of the hydrated calcium silicate board FRMs after exposure to 1000 °C. Scale bars indicate 500 µm and 200 µm lengths, respectively.

Thermal Conductivity

Results for the experimental and theoretical model-based thermal conductivities of the two FRMs are provided in Figures 5 to 8. Error bars on the Hot Disk data indicate ± one standard deviation, typically obtained in eight replicate measurements. In the legends, values in parentheses indicate the value of k_{solid} in units of W/(m·K) used in applying each of the three theories. For each FRM, separate plots are provided for the results obtained during the heating and cooling phases of the measurement cycle described previously. For the cooling phase results, experimental results previously obtained on these same two materials using a newly developed "slug calorimeter" measurement technique are also presented for comparison purposes [9; 19]. In applying the theories of Russell, Frey, and Bruggeman, the value of k_{solid} used in each theory was adjusted (as indicated in the Figure legends) to provide the best fit to the original room temperature thermal conductivity measured for FRM L. While the values used in the Russell and Frey theories, 0.7 and 0.72, respectively, are quite similar, the value needed in the Bruggeman theory is substantially higher (0.95). Previously in the literature [3], by assuming a simple parallel model for heat transfer through the calcium silicate boards, a value of 1.0 W/(m•K) had been estimated for k_{solid}. For both materials, exposure to a 1000 °C temperature produced room temperature (23 °C) thermal conductivities about 5 % lower than those measured on the original

material, likely due to a decrease in density (increase in porosity). Conversely, at 400 °C, after the high temperature exposure, a slight increase in thermal conductivity was observed, likely due to enhanced radiation in the exposed material as a result of its higher porosity and possibly larger pore sizes (lower density and microstructure damage as noted in Figure 4). These results confirm that both porosity and pore size play an important role in the temperature-dependent thermal conductivities of these insulation materials.

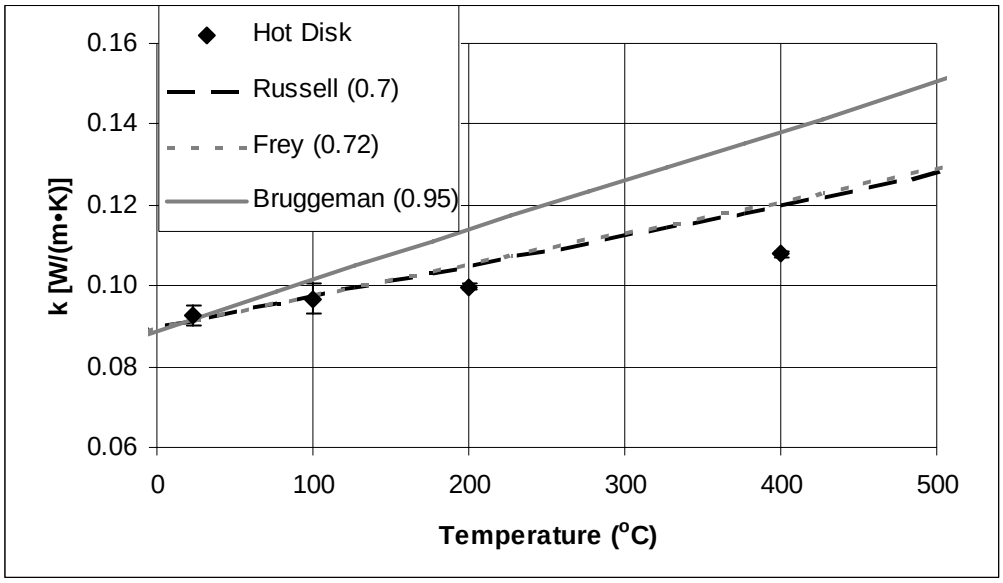

Figure 5. Measured and predicted thermal conductivities for FRM L heated in steps from room temperature to 400 °C.

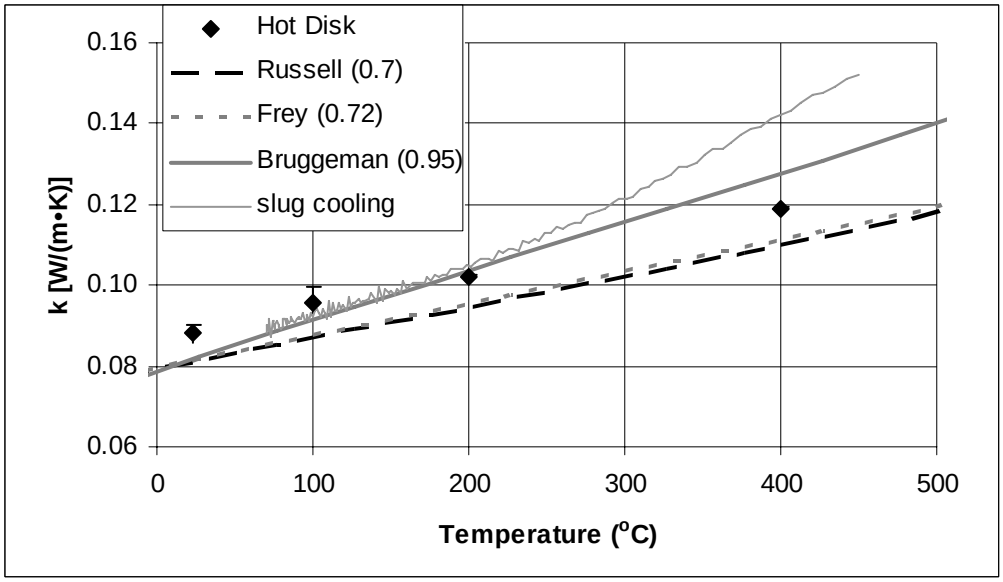

Figure 6. Measured and predicted thermal conductivities for FRM L cooled in steps from 400 °C to room temperature. The specimens were conditioned at 1000 °C prior to measurement. Slug cooling data is from reference [9].

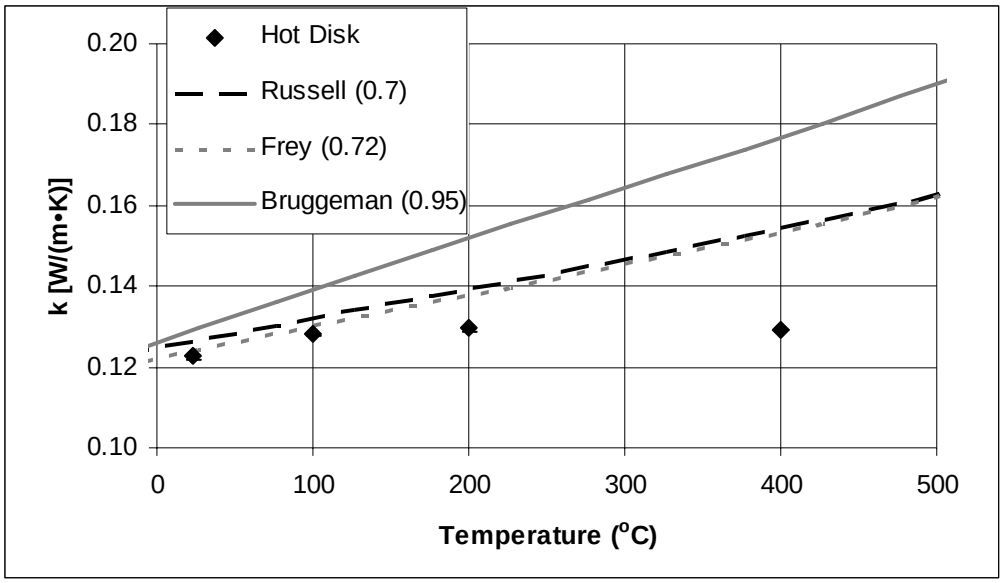

Figure 7. Measured and predicted thermal conductivities for FRM M heated in steps from room temperature to 400 °C.

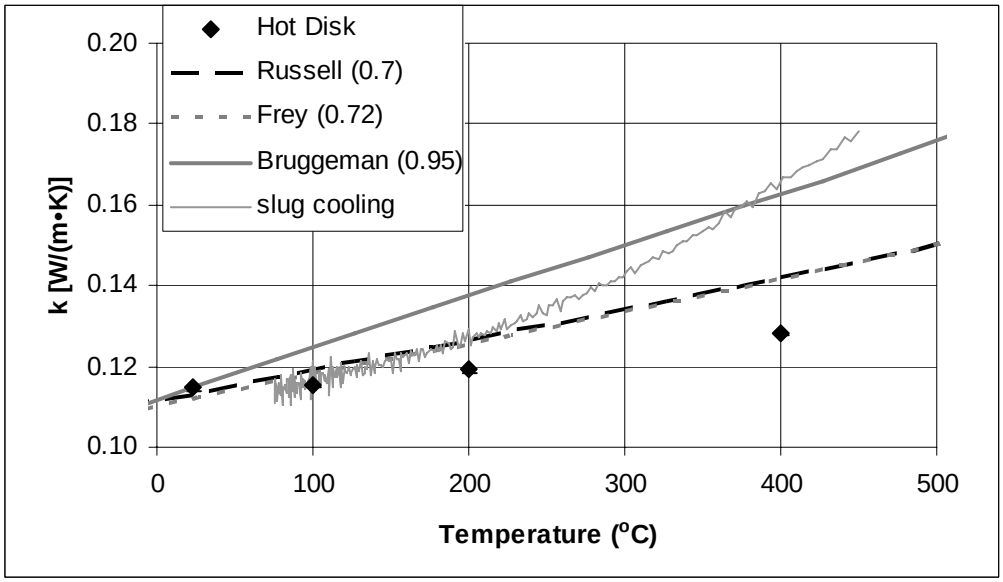

Figure 8. Measured and predicted thermal conductivities for FRM M cooled in steps from 400 °C to room temperature. The specimens were conditioned at 1000 °C prior to measurement. Slug cooling data is from reference [9].

It can be noted in Figures 5 to 8 that the theories of Russell and Frey provide quite similar predictions for the thermal conductivity values and that these two theories generally capture the trends observed in the experimental data better than the theory of Bruggeman. For both materials, the results measured at 200 °C and 400 °C during the heating phase are consistently lower than the predicted values, perhaps indicating that a true equilibrium had yet to be achieved within the FRM materials during their exposure to these temperatures. Also, some physical damage (delamination) to the mica-based Hot Disk sensors was observed after repeated testing at

400 °C, which could have influenced the measurements performed at this highest temperature used in the current study.

For both materials, there is reasonable agreement between the previously performed slug calorimeter and the current Hot Disk measurements for temperatures of 200 °C and lower. At 400 °C, the slug calorimeter measurement values are significantly higher than the Hot Disk ones. In addition to the issues in making Hot Disk measurements at 400 °C that were mentioned earlier, another consideration could be the fact that the values obtained during the slug calorimeter test are reported for a mean specimen temperature, while a temperature gradient of up to 150 °C exists across the 25 mm thick sample (at a mean temperature of 400 °C) for instance. Conversely, the Hot Disk measurements are obtained with a small energy excitation for a sample that has hopefully achieved spatial thermal equilibrium at 400 °C. However, an analysis conducted according to the procedures outlined in the ASTM C1045 Standard Practice for Calculating Thermal Transmission Properties Under Steady-State Conditions [20] indicates that, for these materials' thermal conductivities and the above-mentioned temperature gradients, the effect of the 150 °C temperature gradient is not significant.

Conclusions

The thermal conductivities of calcium silicate boards have been observed to be a function of both temperature and prior exposure history. After exposure to 1000 °C, the room temperature thermal conductivities of both materials examined in this study decreased by about 5 %, while the conductivities measured at 400 °C increased. The observed increases in thermal conductivity with increasing temperature were better described by the theories of Russell and Frey than by that of Bruggeman. Measurements at 400 °C using the Hot Disk equipment were complicated by the slow approach to thermal/hygral equilibrium of these materials and the durability of the higher temperature nickel/mica sensors.

Acknowledgements

The authors would like to thank Mr. John Winpigler of the Building and Fire Research Laboratory (BFRL) for assisting with the powder density measurements. Chi Do would also like to thank the NIST Summer Undergraduate Research Fellowship (SURF) program for providing him the opportunity to work on this project.

References

1. Roels, S., Carmeliet, J., Hens, H., Adan, O., Brocken, H., Cerny, R., Pavlik, Z., Hall, C., Kumaran, K., Pel, L., and Plaage, R. (2004). Interlaboratory Comparison of Hygric Properties of Porous Building Materials, *Journal of Thermal Envelope and Building Science*. 27(4):307-325.

2. Hamilton, A. and Hall, C. (2005). Physicochemical Characterization of a Hydrated Calcium Silicate Board Material, *Journal of Building Physics*. 29(1): 9-19.

3. Koronthalyova, O. and Matiasovsky, P. (2003). Thermal Conductivity of Fibre Reinforced Porous Calcium Silicate Hydrate-Based Composites, *Journal of Thermal Envelope and Building Science*. 27(1): 71-89.

4. Koronthalyova, O. and Matiasovsky, P. (2003). Thermophysical Parameters of Calcium Silicate Insulation Measured by Guarded Hot Plate and Pulse Transient Methods, In: *Thermophysics 2003: Proceedings of the Thermophysical Working Group*. Slovak Physical Society, 39-45.

5. Russell, H.W. (1935). Principles of Heat Flow in Porous Insulators, *Journal of the American Ceramic Society*. 18(1):1-5.

6. Frey, S. (1932). Uber Die Elektrische Leitfahigkeit Binarer Aggregate, *Zeitschrift Fur Elektrochemie*. 38:260-274.

7. Bruggeman, D. (1935). Dielectric Constant and Conductivity of Mixtures of Isotropic Materials, *Annalen Der Physik*. 24(7):636-664.

8. ASTM (1995). ASTM C 188-95 Standard Test Method for Density of Hydraulic Cement, 04.01.

9. Bentz, D.P. (2007). Combination of Transient Plane Source and Slug Calorimeter Measurements to Estimate the Thermal Properties of Fire Resistive Materials, *ASTM Journal of Testing and Evaluation.* 35(3).

10. Taylor, B.N. and Kuyatt, C.E. (1994). Guidelines for Evaluating and Expressing the Uncertainty of NIST Measurement Results, *NIST Technical Note 1297*.

11. Struble, L.J. and Stutzman, P.E. (1989). Epoxy Impregnation of Hardened Cement for Microstructural Characterization, *Journal of Materials Science Letters*. 8(6):632-634.

12. (2006). ImageJ, NIH available at http://rsb.info.nih.gov/ij/ (access verified 01/07).

13. Sahagian, D.L. and Proussevitch, A.A. (1998). 3D Particle Size Distributions From 2D Observations: Stereology for Natural Applications, *Journal of Volcanology and Geothermal Research*. 84(3):173-196.

14. Gustafsson, S.E. (1991). Transient Plane Source Techniques for Thermal Conductivity and Thermal Diffusivity Measurements of Solid Materials, *Review of Scientific Instruments*. 62(3): 797-804.

15. Log, T. and Gustafsson, S.E. (1995). Transient Plane Source (TPS) Technique for Measuring Thermal Transport Properties of Building Materials, *Fire and Materials*. 19(1):43-49.

16. Weast, R.C. (Ed.) (1987). *CRC Handbook of Chemistry and Physics*, CRC Press, Boca Raton, FL.

17. Holman, J.P. (1981). *Heat Transfer*, McGraw-Hill, New York.

18. Loeb, A.L. (1954). Thermal Conductivity: VIII, A Theory of Thermal Conductivity of Porous Materials, *Journal of the American Ceramic Society*. 37(2):96-99.

19. Bentz, D.P., Flynn, D.R., Kim, J.H., and Zarr, R.R. (2006). A Slug Calorimeter for Evaluating the Thermal Performance of Fire Resistive Materials, *Fire and Materials*. 30(4): 257-270.

20. ASTM (2001). ASTM C 1045-01Standard Practice for Calculating Thermal Transmission Properties Under Steady-State Conditions.